

Intracluster gas pressure, entropy injection and redshift evolution

Biman B. Nath^{1*}, Subhabrata Majumdar^{2†}

1. Raman Research Institute, Sadashiva Nagar, Bangalore 560080, India

2. Department of Theoretical Physics, Tata Institute of Fundamental Research, 1 Homi Bhabha Road, Mumbai 400005, India

30 September 2018

ABSTRACT

We study the effect of entropy injection in the intracluster medium (ICM) in light of the recent observationally determined universal pressure profile of the ICM. Beginning with a power-law entropy profile that is expected in the absence of any feedback, we show that a simple universal prescription of entropy injection results in the final, observed universal pressure profile. This simple prescription has two components, one associated with an overall increase in entropy and another associated with injection in the central parts of the cluster. Importantly, both the components of entropy injection are needed to produce the final universal pressure profile. This is indicative of a need of both preheating the ICM as well *in situ* AGN/SNe heating. We demonstrate the usefulness of the method by extending the calculations to clusters at high redshift, and predict redshift evolution of cluster scaling relations that can be tested against data. We show that the self-similar evolution of the universal pressure profile is equivalent to a negative evolution of entropy injection with redshift, with a scaling $S_{inj} \propto (1+z)^{-0.8} S_{inj}(z=0)$. We also show the current observational data is indicative of the entropy injection decreasing with redshift.

Key words: galaxies: cluster:general – galaxies: intergalactic medium – X-rays:galaxies:clusters – cosmology:miscellaneous

1 INTRODUCTION

Galaxy clusters are being increasingly used as cosmological probes. The evolution of galaxy cluster abundances, for example, is sensitive to the values of cosmological parameters, and have been extensively studied in order to determine or constrain these parameters (Wang & Steinhardt 1998, Holder et al. 2001, Majumdar & Mohr 2003, 2004, Gladders et al. 2007, Vikhlinin et al. 2009, Rapetti et al. 2009, 2010, Rozo et al. 2010, Sartoris et al. 2010). These attempts have been, however, limited by the inadequacy of our knowledge of the state of the intracluster medium (ICM) of clusters. Cluster scaling relations show that the distribution of the ICM gas is different from simple models of cluster formation in which baryonic gas only reacts to the gravitational potential of the dark matter (Benson et al. 2004, da Silva et al. 2004, Bonaldi et al. 2007, Bonamente et al. 2008).

It is now believed that a number of non-gravitational processes may have affected the ICM gas, including radiative cooling and energetic feedback from active galactic nuclei

(AGN) and/or supernovae (for example, see Voit & Bryan 2001, Nath & Roychowdhury 2001, Balogh et al. 2001, Borgani et al. 2004, Roychowdhury et al. 2004, Kravtsov et al. 2005, Puchwein et al. 2008, Battaglia et al. 2010). These processes tend to raise the entropy of the ICM gas, essentially heating the gas and pushing it outward, and they make the gas less X-ray bright for a given temperature, and help in reconciling theoretical predictions with observed data.

In recent years, the Sunyaev-Zel’dovich (SZ) temperature distortion of the cosmic microwave background radiation (CMBR) has received a lot of attention, in light of the possibility of observing a large number of clusters through SZ effect, since the magnitude of the effect is independent of redshift (Birkinshaw 1999). The scaling relations for SZ effect is also altered by the non-gravitational processes mentioned above, and in general the magnitude of the SZ effect is decreased by the non-gravitational processes mentioned above (White, Hernquist & Springel 2002, Roychowdhury, Ruszkowski & Nath 2005).

Recently, a universal pressure profile for the ICM gas has been shown to fit the X-ray observations of clusters (Arnaud et al. 2010). This pressure profile can be combined with a mass model for the dark matter halo to yield the corre-

* biman@rri.res.in

† subha@tifr.res.in

sponding gas density and temperature profiles, and therefore its entropy profile. In this paper, we compare this entropy profile of the ICM (inferred from the observed universal pressure profile) to determine the additional entropy needed for the ICM gas, starting with a physically motivated profile that is expected in the absence of any feedback. The aim is to determine the additional entropy needed to explain the observations of local clusters in a phenomenological manner.

We then speculate upon the possible evolution of entropy injection with redshift, and calculate the corresponding pressure profiles at high redshift. These profiles can be tested against the data for the evolution of cluster scaling relations with redshift (e.g. between X-ray luminosity and temperature), and the evolution of entropy injection with redshift can be inferred with the help of this method. We show that although present available data are insufficient to constrain the evolution of entropy injection, one will be able to iterate with better data in future and determine the entropy injection at high redshift from observed cluster scaling relation evolution.

The rest of the paper is structured as follows: In §2, we show different ways to calculate the ICM pressure profiles, in §3 we model injected entropy, in §4 we look at its evolution with redshift and we finally conclude in §5. Throughout the paper, we use the subscript U for physical parameters related to the universal pressure profile by Arnaud et al. (2010). Also, we use the subscripts i and f for initial and final profiles and values.

2 ICM PRESSURE PROFILE

Recent observations by Arnaud et al. (2010) have shown that a scaled universal profile for the pressure of the ICM can fit the X-ray observations. Defining $x = r/R_{500}$, where R_{500} is the radius within which the mean over density is 500 with respect to the critical density, this profile is given by (eqns 9, 11, 13 of Arnaud et al. 2010),

$$P_U(x) = P_{500} \frac{P_0 h_{0.7}^2}{(c_{500}x)^\gamma [1 + (c_{500}x)^\alpha]^{(\beta-\gamma)/\alpha}} \quad (1)$$

where,

$$\begin{aligned} P_{500} (\text{keV cm}^{-3}) &= 1.65 \times 10^{-3} E(z)^{8/3} \\ &\times \left[\frac{M_{500}}{3 \times 10^{14} h_{0.7}^{-1} M_\odot} \right]^{2/3 + \alpha_p + \alpha'_p(x)}, \\ P_0 &= 8.403 h_{0.7}^{-3/2}, \end{aligned} \quad (2)$$

where $c_{500} = 1.177$, $\alpha = 1.051$, $\beta = 5.4905$, $\gamma = 0.3801$, $\alpha_p = 0.12$, $\alpha'_p(x) = 0.1 - (\alpha_p + 0.1) \frac{(x/0.5)^3}{1 + (x/0.5)^3}$, M_{500} is the mass enclosed within R_{500} , $H = 70 h_{0.7} \text{ km s}^{-1} \text{ Mpc}^{-1}$, and $E(z) = H(z)/H_0 = [\Omega_0(1+z)^3 + \Lambda_0]^{1/2}$, is the ratio of the Hubble constant at redshift z to its present value.

We assume a Navarro-Frenk-White (NFW) profile for the dark matter distribution (Navarro et al. 1997), along with an estimation of the concentration parameter ' c ' from observations by Comerford & Natarajan (2007), given by $c_{vir} = \frac{14.5 \pm 6.4}{1+z} (M_{vir}/1.3 \times 10^{13} h^{-1} M_\odot)^{-0.15 \pm 0.13}$. We note that this prescription refers to the total cluster mass and is an empirical one. However, we have found that our final results are largely insensitive to the assumptions of the

concentration parameter (see also Chaudhuri & Majumdar 2011).

We also use the analytical fit by Bryan & Norman (1988) for the over density $\Delta_c(z) = 18\pi^2 + 82x - 39x^2$, with $x = \Omega_m(z) - 1$, with which one can calculate the virial radius, as,

$$r_{vir} = \left(\frac{M_{vir}}{(4\pi/3)\rho_{crit}(z)\Delta_c(z)} \right)^{1/3}. \quad (3)$$

In order to determine the additional entropy we need to use a default profile for the ICM gas that is predicted in the absence of any energy input. Following the tradition in X-ray astronomy, we define the 'entropy', S as $k_B T/n_e^{2/3}$ (which is usually expressed in the units of keV cm^2).

There are three possibilities in this regard:

- (a) One can either use an entropy profile that one expects from the consideration of ICM gas getting heated at the accretion shock, and in the absence of radiative cooling. Voit et al. (2005) showed that simulations with only gravitational processes yield a power law entropy profile of type $S_i(r) = 1.32 \times S_{200} (r/R_{200})^{1.1}$, where

$$S_{200} = \frac{\mu \mu_e^{2/3} m_p^{5/3}}{2} \left[\frac{2\pi G^2 M_{200}}{15 f_b H(z)} \right]^{2/3}. \quad (4)$$

Here, we use an equivalent expression that uses R_{500} , taken from Pratt et al. (2010), using the observed mean value of $c_{500} = 3.2$ for relaxed clusters (Pointecouteau et al. 2005),

$$S(r)/S_{500} = 1.42(r/R_{500})^{1.1} \quad (5)$$

where

$$S_{500} = 106 \text{ keV cm}^{-2} \left[\frac{M_{500}}{10^{14} h_{0.7}^{-1} M_\odot} \right]^{2/3} \left(\frac{1}{f_g} \right)^{2/3} E(z)^{-2/3} h_{0.7}^{-4/3}, \quad (6)$$

f_g being the baryon fraction. This assumes a metallicity of $0.3 Z_\odot$ and a mean molecular weight $\mu = 0.596$. This profile appears to fit the results of simulations without radiative cooling, with approximately 20% dispersion, especially beyond $r \geq 0.1 R_{200}$ (see also Mitchell et al. 2009).

Assuming the initial gas distribution to have this entropy profile, $S_i(r)$, and assuming this gas to be in hydrostatic equilibrium with a given total mass profile, the initial gas pressure profile, $P_{g,i}(r)$ can be obtained from,

$$\begin{aligned} \frac{dP_{g,i}}{dM_g} &= -\frac{GM(\leq r)}{4\pi r^4} \\ \frac{dr}{dM_g} &= \frac{1}{4\pi r^2 (\mu^{3/5} \mu_e^{2/5}) m_p} \left[\frac{P_{g,i}}{S_i(r)} \right]^{-3/5}, \end{aligned} \quad (7)$$

where $M(\leq r)$ is the total mass inside radius r , given by the NFW profile, and $M_g(r)$ is the gas mass inside r . These equations can be solved with the boundary conditions that $M_g = 0$ at $r = 0$, and that the total gas fraction inside the virial radius, $M_g(r_{vir})/M_{vir} = \Omega_b/\Omega_m$.

- (b) Simulations that include radiative cooling, however, can also be used to obtain an initial profile that we can compare with the observed profile in order to determine the additional entropy needed. Loken et al. (2002) found from simulations with cooling a universal temperature profile in the range $0.04 < r/r_{vir} < 1$, given by,

$$T_i(r) = \frac{1.33 \langle T \rangle}{(1 + (1.5r/r_{vir}))^{1.6}}, \quad (8)$$

where $\langle T \rangle$ is the emission weighted temperature of the cluster gas. We use an empirically derived scaling relation to determine this temperature, from the observations of Finoguenov et al. (2001), (although there may be an order unity difference between these two definitions of emission weighted temperature)

$$M_{500} = (2.64^{+0.39}_{-0.34}) 10^{13} M_{\odot} \left(\frac{k_b \langle T \rangle}{1 \text{ keV}} \right)^{1.78}. \quad (9)$$

We can then compute the initial gas density profile assuming the gas to be in hydrostatic equilibrium and using the above mentioned temperature profile,

$$\frac{1}{\rho_{g,i}(r)} \frac{d}{dr} \left[\frac{\rho_{g,i} k_B T_i}{\mu m_p} \right] = - \frac{GM(\leq r)}{r^2}. \quad (10)$$

The gas fraction within the virial radius is assumed to be equal to the cosmic baryon fraction, Ω_b/Ω_m . The inferred gas density and temperature profiles can then be used to derive the initial entropy profile $S_i(r) = k_b T_i / (\rho_{gas,i} / (\mu_e m_p))^{2/3}$.

• (c) One can also use a profile with a polytropic equation of state, $P \propto \rho^\Gamma$. Li et al. (2010) has recently used this as a fiducial profile, with $\Gamma = 1.2$. The normalization comes from the assumption of total gas fraction within the virial radius to be same as the cosmic gas fraction, as in the above models.

The initial pressure profiles resulting from these three possible initial entropy profiles can be compared with the observed universal pressure profile of Arnaud et al. (2010). Given the observed pressure profile, one can get to density, temperature and entropy profile, by assuming hydrostatic equilibrium. We determine the gas density profile, $\rho_{g,U}(r)$, using hydrostatic equilibrium condition and the observed universal pressure (eqn 1),

$$\frac{1}{\rho_{g,U}(r)} \frac{dP_U(r)}{dr} = - \frac{GM(\leq r)}{r^2}. \quad (11)$$

We note that the observed pressure profile refers only to electron pressure and we should multiply the electron pressure $P_e = n_e k T_e$, by the ratio of μ_e/μ , where $\mu(= 0.59)$ is the mean molecular weight, and $\mu_e(= 1.14)$ is the mean molecular weights per free electron, their values being appropriate for a gas with metallicity of $0.3 Z_{\odot}$.¹

Once the gas density profile is calculated, the corresponding temperature profile is then readily computed as $T_U(r) = P_U(r) / (k_b \rho_{g,U}(r) / (\mu m_p))$, and then the entropy profile, $S_U(r) = k_B T_U(r) / (\rho_{g,U}(r) / (\mu_e m_p))^{2/3}$.

We show in Figure 1 the three initial entropy profiles for a given cluster mass: the case of universal temperature profile (dashed line), that of a polytropic equation of state with $\Gamma = 1.2$ (dot-dashed line), and the scaled entropy profile of Voit et al. (2005) (dotted line). The solid curve shows the entropy profile corresponding to the observed universal pressure profile of Arnaud et al. (2010). As expected, the computed initial profile using radiative cooling (dashed line) has a higher entropy than the power-law profile expected without cooling (dotted line). It should be noted that these curves should be used only for $\text{Log}_{10}[r/r_{vir}] \geq -1.5$, where

¹ The total pressure, assuming a common temperature, $P = kT \sum_i n_i = kT n_e \frac{\sum_i n_i}{n_e} = P_e \frac{\sum_i m_i n_i / n_e}{\sum_i m_i n_i / \sum_i n_i} = P_e \frac{\mu_e}{\mu}$.

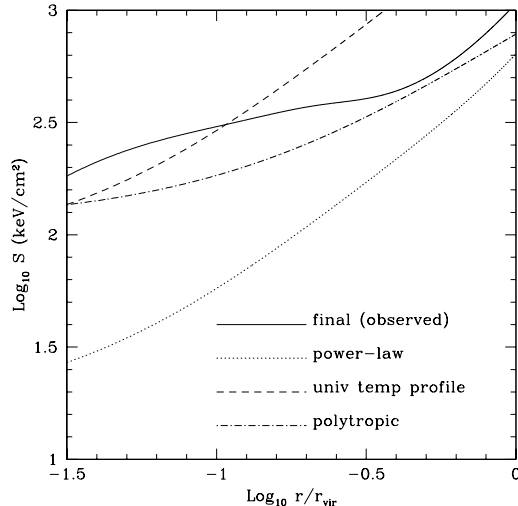


Figure 1. The entropy profile of ICM gas, for $M_{\text{vir}} = 10^{14} h^{-1} M_{\odot}$. The solid line shows the entropy profile corresponding to the observed universal pressure profile of Arnaud et al. (2010). The dotted line shows the scaled power-law entropy profile from Voit et al. (2005), the dashed line shows the initial profile computed using the universal temperature profile of Loken et al. (2002), and the dot-dashed line shows the entropy profile corresponding to a polytropic gas with $\Gamma = 1.2$.

the observational data are more secure than in the inner regions. We can see that the inferred entropy at $r \sim 0.1 r_{vir}$ is several times higher than the one expected from purely adiabatic case.

Given these choices for the initial entropy profile, we choose the one with power-law entropy, of Voit et al. (2005), for the following reasons. Firstly, the polytropic gas profile lacks physical motivation, since it is not clear why the ICM gas should behave in a polytropic manner in the absence of feedback. Secondly, although the universal temperature profile from radiative simulations is an appealing choice, it is not clear as to what extent it depends on the parameters used in the simulations, and also its possible redshift variation is unclear. On the contrary, the power-law entropy profile is simple and rests on basic assumptions for the behaviour of gas in a gravitational potential well.

3 INJECTED ENTROPY

Next we compute the additional injected entropy needed to reconcile the initial profiles with the observed ones. The extra entropy can be expressed in different ways depending on the manner in which entropy is injected into the ICM. Previous workers have characterized the additional entropy as a constant entropy 'floor' that is independent of the radius. For example, Li et al. (2010) have recently used a value of $S_{inj} \sim 100\text{--}200 \text{ keV cm}^{-2}$ to determine the ICM pressure profile for their calculation of the SZ effect. This choice of characterizing the injected entropy is motivated by the curves showed in Figure 1, in which the gas at lower radius appears to have an entropy 'floor'.

There is, however, one problem with this characterization. When one adds entropy to the initial profile, the gas shells move outward. In other words, entropy added at one

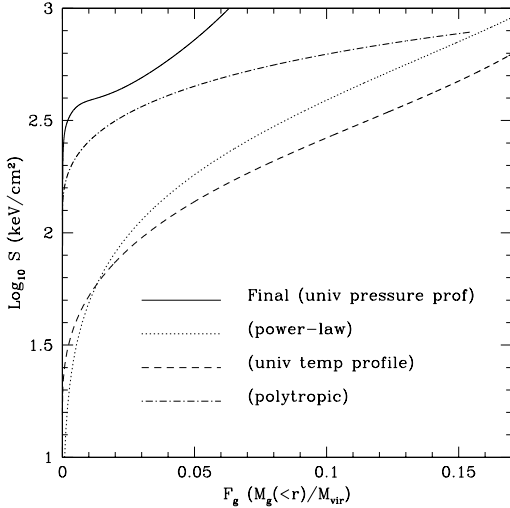


Figure 2. Same as in Figure 1 except that the profiles are plotted against the gas fraction F_g instead of the radial coordinate.

position is carried elsewhere by the movement of the gas, and so the comparison of final and initial entropies at a given radial position does not remain physically significant. As Li et al. (2010) have also recently noted, the injected entropy should be characterized by the gas shell in which the injection has occurred. In other words, one should compare $S_f(F_g)$ with $S_i(F_g)$, where $F_g(r) = M_g(\leq r)/M_{\text{vir}}$ is the gas fraction inside a radius r . Note that this gas fraction is different from the usual definition of gas fraction in the literature, $f_g = M_g(r)/M(\leq r)$; we distinguish these two distinct parameters by using two different notations for them.

We show in Figure 2 the corresponding entropy profiles, as functions of F_g , for $M_{\text{vir}} = 10^{14} h^{-1} M_{\odot}$. It is clear that the observed profile (solid line) corresponds to a case where the gas fraction within r_{vir} has decreased from the initial value $\Omega_b/\Omega_m \sim 0.16$, implying outward movement of gas shells. The entropy ‘floor’ that appears in the entropy profile in radial direction exists here only for the very inner shells of gas. For most of the gas in the cluster, the (logarithm of) final entropy (solid line) is approximately separated from the initial profiles by an additive factor, which translates to a multiplicative factor for entropy. Viewed in this way, in terms of entropy injection in Lagrangian gas shells, we find it useful to characterize the entropy injection as a combination of an ‘entropy floor’ and a multiplicative factor for the initial profile: $S_f(F_g) = S_c + \eta S_i(F_g)$.

The two terms have different physical implications. Note that the entropy ($S = kT/n_e^{2/3}$) used here is proportional to the *logarithm* of gas entropy. If there had been no constant term (S_c), then we could write the excess energy per particle as $\Delta\epsilon$, and the entropy $s = \text{Const} \times \ln S$, then we have $\Delta\epsilon = T\Delta s \propto T \frac{\Delta S}{S} \propto T(\eta - 1)$. Here, since the temperature is a weak function of radius, a constant η would imply a near uniform injection of energy.

On the other hand, if the entropy injection were to be only characterized with a constant term, then we would have $\Delta\epsilon \propto T \times S_c/S_i \propto n_i^{2/3}$, which would imply that energy feedback works mostly in the inner regions where the gas density is highest. Our adopted characterization, with a constant

term and a multiplicative factor essentially allows provisions for both these modes of energy feedback.

In order to determine the level of entropy injection (namely, the value of η), we solve the following equations for hydrostatic equilibrium for the final gas profile:

$$\begin{aligned} \frac{dr}{dF_g} &= \frac{M_{\text{vir}}}{4\pi r^2 \mu m_p} \left(\frac{P_f}{S_f k_b} \right)^{-3/5} \\ \frac{dP_f}{dF_g} &= -\frac{GM(\leq r) M_{\text{vir}}}{r^2 4\pi r^2}, \end{aligned} \quad (12)$$

where $F_g = M_g(r)/M_{\text{vir}}$.

The three variables to be determined here are η , $P_f(r)$, $F_g(r)$, and we need three boundary conditions to solve these equations. One is an obvious choice: (1) $F_g(r=0) = 0$. (2) Another obvious choice is that $P_f(R_{500}) = P_U(R_{500})$, so that the final pressure profile corresponds to the observed universal pressure profile. (3) Lastly we use the value of gas fraction at an outer radius, but this requires an explanation.

For the third boundary condition, we use the value of $F_g(R_{500})$ (i.e., $M_g(R_{500})/M_{\text{vir}}$) that corresponds to the universal pressure profile. We note that the gas fraction at R_{500} as given by the universal pressure profile is different from the ratio of $\Omega_b/\Omega_m \sim 0.167$, which implies that a fraction of the original ICM gas has been thrown out of the system, if one considers the ratio Ω_b/Ω_m to be universal initially. We show in Figure 3 the gas fraction implied by the universal pressure profile, and compare with other observations. Note that observations of gas fraction within R_{500} usually refers to $f_g(R_{500}) = F_g(R_{500}) \times (\frac{M_{\text{vir}}}{M(<R_{500})})$. In Figure 3 we show the values of $f_g(R_{500})$ as given by the universal pressure profile (solid line) for clusters at $z=0$ and compare them with the observed values (dotted line), as reported by Sun et al. (2009).

We also show by the dashed line another ratio, that of the gas mass within a radius $2R_{\text{vir}}$ and the total virial mass of the cluster. This ratio, $F_g(2R_{\text{vir}}) = \frac{M_g(2R_{\text{vir}})}{M_{\text{vir}}}$, is found to be *almost a constant* for all clusters, and close to the value of Ω_b/Ω_m , shown by the dot-dashed line, with an average deviation of order $\sim 10\%$. This interesting result suggests that a fraction of the ICM gas, originally inside R_{vir} and with a universal gas fraction of Ω_b/Ω_m , gets ejected due to the feedback process, but that the gas does not extend beyond a radius $2R_{\text{vir}}$.

Entropy feedback predominantly affects the gas while keeping the dark matter unchanged. In this case, gas mass conservation will ensure that $M_g(R_{\text{vir}}, i) = M_g(2R_{\text{vir}}, f)$, where the latter term is the gas mass within $2R_{\text{vir}}$ after the feedback processes. Dividing both sides by M_{vir} , and recalling that the initial profile is normalized by $M_g(R_{\text{vir}}, i)/M_{\text{vir}} = \Omega_b/\Omega_m$, yields the condition for the final profile, $M_g(2R_{\text{vir}})/M_{\text{vir}} = \Omega_b/\Omega_m$. The choice of the final radius to be $2R_{\text{vir}}$ is slightly arbitrary. However, this choice is consistent with the findings of Battaglia et al. 2010, who show that there is significant contribution to the SZ flux from beyond the virial radius, and going beyond $2R_{\text{vir}}$ does not add to the SZ power. This result allows us to use a boundary condition, that the gas fraction $F_g(2R_{\text{vir}}) = \frac{M_g(2R_{\text{vir}})}{M_{\text{vir}}} \sim \Omega_b/\Omega_m$. We also show in Figure 3 by two thin dashed lines the results for $F_g(2.5R_{\text{vir}})$ and $F_g(1.5R_{\text{vir}})$, and the total spread is of order 17% of the

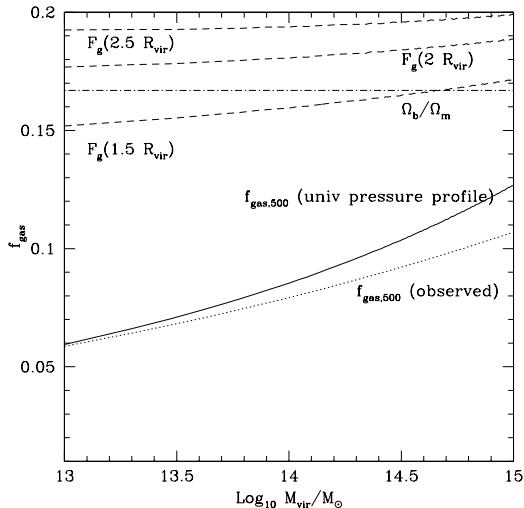


Figure 3. Gas fraction within R_{500} ($f_g = M_g(R_{500})/M(R_{500})$) is plotted as a function of cluster virial mass, for the universal pressure profile (solid curves), for $z = 0$. The dotted line shows the observations of Sun et al. (2009) and the dot-dashed line shows the value of Ω_b/Ω_m . The topmost (solid) dashed line shows the fraction $F_g(2R_{vir})$, which is the ratio $M_g(2R_{vir})/M_{vir}$, as computed from extending the universal pressure profile to $2R_{vir}$. Interestingly, this line is close to the Universal gas fraction to within 10 – 15% for all masses. The pair of thin dashed lines above and below this curve are for $F_g(2.5R_{vir})$ and $F_g(1.5R_{vir})$, respectively.

values of $F_g(2R_{vir})$. This is the level of uncertainty in our results that stems from the lack of precise knowledge about the outer boundary condition.

We find that with the above mentioned assumptions and boundary conditions, the following prescription of entropy injection works satisfactorily in converting the initial entropy profile to the final profile as given by the universal pressure profile at $z = 0$, for $10^{14} \leq M_{vir}/M_\odot \leq 10^{15}$:

$$S_{inj}(F_g) = 200 \text{ keV cm}^{-2} + 2 \times \left(\frac{M_{vir}}{10^{14} h^{-1} M_\odot} \right)^{-0.2} \times S_i(F_g). \quad (13)$$

The values of the coefficients provide the best match within an accuracy of $\sim 15\%$. This form of the feedback implies that low mass clusters need overall more feedback than rich clusters, although (from the constant term) all clusters appear to need feedback in their central regions.

Physically these two modes may refer to preheating and AGN/SN feedback processes, one in which all the gas particles in the ICM are energized and another, in which particles in the central region get more entropy than elsewhere. We show below that from the comparison of the final pressure profile and the initial pressure profiles, that it would be impossible to achieve the final pressure profile with only a single mode of entropy injection.

We show in Figures 4 and 5 two examples of the result of this type of entropy injection, for $M_{vir} = 10^{15} h^{-1} M_\odot$ and $M_{vir} = 10^{14} h^{-1} M_\odot$, respectively, at $z=0$. The top-left panels of both figures show the density profiles: dashed lines show the initial profile of power-law entropy; the dot-dashed lines show the profile corresponding to the universal pressure profile and the dotted lines show the final profile, which is a result of the entropy injection according to the

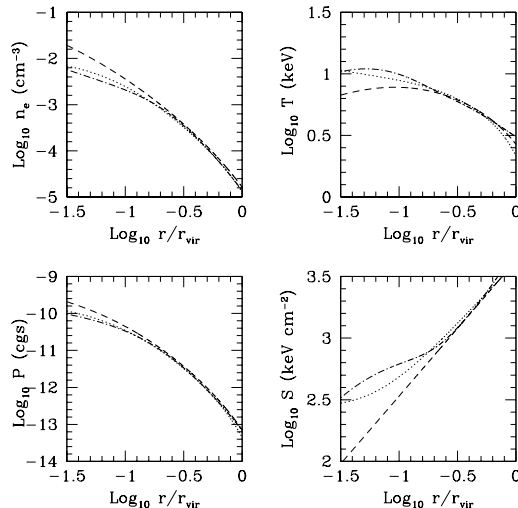


Figure 4. Comparison between the initial and final profiles, before (dashed) and after (dotted) entropy injection, and those obtained from universal pressure profile (dot-dashed), for $M_{vir} = 10^{15} h^{-1} M_\odot$. The top-left panel shows the density profiles, the top-right panel shows the temperature profiles, the bottom-left panel shows the pressure profiles and the bottom-right panel shows the entropy profiles.

above mentioned prescription. The top-right panels show the temperature profile, the bottom-left panels show the pressure profile and the bottom-right panels show the entropy profiles.

Before discussing the results, let us summarize the method of our calculation. We have began with a power-law entropy profile, and used a prescription for entropy injection, which along with the above mentioned boundary conditions yield a pressure profile. We iterate a loop until the three boundary conditions are matched (within 10%). This leads to a match with the observed universal pressure profile because of the chosen entropy injection prescription (13). As a result, we find in Figures 4 and 5 that the final pressure profiles (bottom-left panels, dotted lines) match well the observed profile (dot-dashed lines). The match for the temperature (top right panels) and entropy (bottom right panels) profiles are less satisfactory, but we note that the dot-dashed lines here are not observed profiles, but inferred from the universal pressure profiles. Since we have decided to peg our boundary conditions on the observed pressure profiles, we conclude that the above entropy injection prescription gives a satisfactory match with observations. *Since a single prescription appears to work for the whole range of cluster masses, one could call it a universal entropy injection prescription.*

4 EVOLUTION WITH REDSHIFT

4.1 Evolution of entropy and pressure

Our exercise has so far been limited to observed clusters at low redshifts: we have used a physically motivated initial gas profile, and compared it to the observed profile to deduce a prescription for entropy injection. It is true that the entropy injection prescription allows us to speculate on

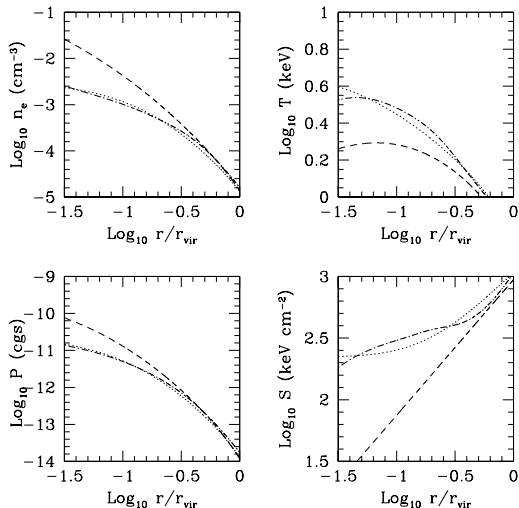


Figure 5. Same as Figure 4a, but for $M_{\text{vir}} = 10^{14} h^{-1} M_{\odot}$.

the kind of feedback process that may give rise to the entropy enhancement. The prescription, however, remains a phenomenological one, and we wish to explore its usefulness beyond the regime within which it has been deduced in the previous section.

In particular, we wish to study the ICM in high redshift galaxy clusters, and determine the amount of feedback that may have occurred at high redshift. The properties of the ICM at high redshift have been studied through the observations of evolution of cluster scaling laws, e.g., the relations between X-ray luminosity and temperature, and with the help of numerical simulations. In the rest of the paper, we show that our semi-analytical formalism can help in this regard, by determining the amount of feedback needed to produce an ICM profile that is consistent with redshift evolution of cluster scaling relations. Voit (2005) had suggested that cluster scaling relations would differ at high redshifts owing to the effects of feedback and radiative cooling (see also Muanwong, Kay & Thomas 2006; Short et al. 2010).

At present, however, the usefulness of this method is limited by the lack of accurate determinations of scaling relation evolutions. Ettori et al. (2004) found that the evolution of $M - T$ relation in a sample of 28 clusters at $0.4 < z < 1.3$ followed the self-similar model, expected from simple cosmological considerations. But they found the normalization of the $L_x - T$ relation to decrease with redshift, which was later confirmed by Hilton et al. (2007) from a study of a high redshift cluster with *XMM - Newton* (see also Branchesi et al. 2007). Morandi et al. (2007) found negative evolution in the $M - T$ relation but a positive evolution for $L_x - T$ relation (see also Maughan et al. 2007). At the same time, Maughan et al. (2006) found little evidence for any such redshift evolution apart from that expected from self-similarity.

One reason for this uncertainty is the scatter produced by the large X-ray luminosity at the centres of cool core clusters (Chen et al. 2007). Cluster mergers also produce deviations (Kravtsov et al. 2006). Also, the sample of small number of clusters at high redshift suffers from selection effects (Pacaud 2007). It is hoped that a large and homogeneous sample will be gleaned from the upcoming XMM

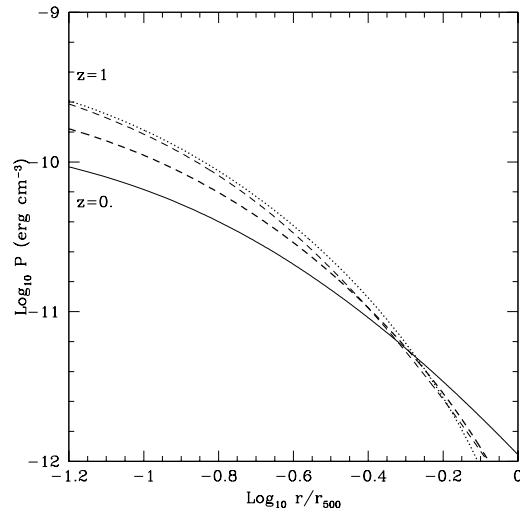


Figure 6. The pressure profiles for $M_{\text{vir}} = 10^{15} h^{-1} M_{\odot}$ at $z = 0$, and 1 are plotted against r/R_{500} (in cgs units), for the case of constant entropy enhancement. The solid line refers to the $z = 0$ profile, and the thick dashed line is for $z = 1$. The thin dashed line show the universal pressure profile scaled by a factor $E(z)^{8/3}$ for comparison. We also show with dotted line the case for the entropy injection scaling as $(1+z)^{-0.8}$, which matches closely the self-similarly scaled universal pressure profile.

Cluster Survey (XCS) (Romer et al. 2001), and allow a better determination of the evolution of X-ray scaling relations.

Keeping these uncertainties in the observed relations in mind, we would like to extend our phenomenological study to high redshift clusters. For this exercise, we need to assume a redshift evolution of the feedback prescription. Also, instead of changing the boundary conditions with redshift, we assume that the boundary conditions at high redshift is the same as at $z = 0$, namely, $F_g(r = 0) = 0$, and that $F_g(2R_{\text{vir}}) = \Omega_b/\Omega_m$. This will yield the gas profiles, which can then be compared with the expectations from scaling relation evolutions. This process can then be iterated to determine the amount of feedback that is required to explain the evolution of the cluster scaling relations. This iteration will make sense with accurate determination of scaling relation evolutions, and in the absence of such observations, we only demonstrate the first part of this process, namely, prediction of ICM at high z corresponding to a given feedback prescription and how this can be used to compare with observed cluster scaling relation evolutions.

We have used simple modifications to the entropy injection prescription. Here, one can work out a number of possibilities, parameterized by a certain set of variables and test the resulting pressure profiles against data. In this paper, we demonstrate the utility of our approach by calculating the cluster scaling relations with redshift resulting from a simple redshift scaling of the entropy injection prescription, namely, $S_{inj}(z) = (1+z)^\alpha S_{inj,z=0}$. This means that we multiply the expression of injected entropy in eqn 13 by a factor $(1+z)^\alpha$.

Assuming this feedback prescriptions, we calculate the ICM profiles for clusters at high redshift for different values of the power-law index α . In Figure 6, we show the resulting pressure profiles for $\alpha = 0$, for $M_{\text{vir}} = 10^{15} h^{-1} M_{\odot}$ at $z = 0$ (thick solid line) and 1 (thick dashed line). The thin

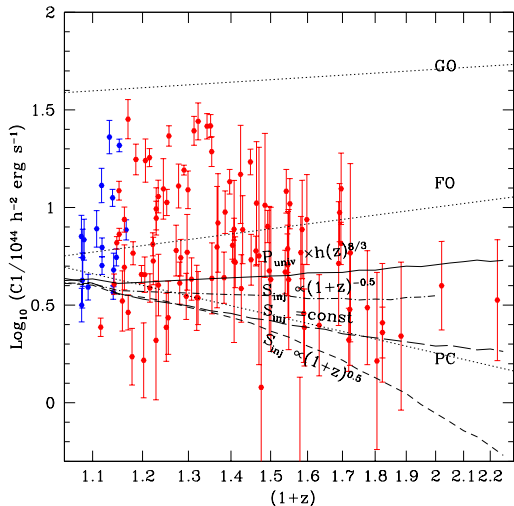


Figure 7. The evolution of the normalization $C1$ of $L_x - T$ relation is shown with redshift, for universal pressure profile with self-similar scaling (solid line) and three cases of enhanced pressure profile: for a constant entropy injection at all redshifts (long dashed line), for $S_{inj} \propto (1+z)^{-0.5}$ (dot-dashed line), and $S_{inj} \propto (1+z)^{0.5}$ (short dashed line). The three dotted lines show the results of simulations GO, FO and PC (see text for details).

line shows the self-similarly scaled universal pressure profile at $z = 1$, scaled by the factor $E(z)^{8/3}$. The resulting profiles clearly have larger values for pressure than those expected from a self-similar evolution of the pressure profile. We can similarly calculate the pressure profiles for other cluster masses and at different redshifts.

We also show in Figure 6 the case of $\alpha = -0.8$, for a negative evolution of entropy injection, at $z = 1$ and we find that this matches the self-similarly scaled universal pressure profile closely. We have checked this at other redshifts $z < 1$ and found that they match within an accuracy of 25%. Our calculations with different values of the parameter α show that the pressure profiles at high redshift are increasingly suppressed with increasing values of α , as expected. This will result in different forms of evolution of various cluster scaling relations, which can be tested against data, and we now turn to a discussion on this issue.

4.2 Evolution of scaling relations

How do these profiles compare with the observations of cluster scaling relations? Following Short et al. (2010), we study the normalizations of the $L_x - T$ and the SZ decrement $Y_x - M$ relation (see below) and their evolution in redshift. For the $L_x - T$ relation, we assume a power-law relation,

$$L_x E(z)^{-1} = C1(T_{sl}/6keV)^\alpha, \quad (14)$$

where L_x is the X-ray luminosity at 0.5 – 1 keV band and T_{sl} is the spectroscopic like temperature, as defined by Mazzotta et al. (2004). One can study the evolution of the normalization $C1$, with redshift, for ICM profiles given by self-similarly scaled universal pressure profile, and those with other forms of evolution.

In Figure 7 we show the redshift evolution of $C1$, in the units of $10^{44} h^{-2} \text{ erg s}^{-1}$. The solid line shows the evolu-

tion obtained from a self-similarly scaled universal pressure profile, which means that the profile is scaled by a factor $E(z)^{8/3}$. The long dashed line shows the case of entropy injection being constant with redshift, the dot-dashed line shows the case of the scaling $(1+z)^{-0.5}$, whereas the short-dashed line shows the results of $S_{inj} \propto (1+z)^{0.5}$.

This figure can be compared with Figure 12 of Short et al. (2010), which shows the results of different simulations and observations. As mentioned earlier, the data has large scatter and the form of evolution remains unclear. Simulations with feedback, however, show either positive evolution (from FO simulation including AGN and supernova feedback, by Short et al. (2010)) or negative evolution (PC simulation, including preheating, by Hartley et al. 2007). Simulations without any feedback (GO, in the Millennium Gas simulations series; see Short et al. 2010) show a mild positive evolution. However, the amplitude without feedback fails to match observations. Thus some form of energy injection is absolutely necessary.

We show in Figure 8 the redshift evolution of the normalization $C2$ of the relation between $Y_x - M_{500}$ relation, normalizing at $M = 5 \times 10^{14} h^{-1} M_\odot$,

$$Y_x E(z)^{-2/3} = C2 \left(\frac{M_{500}}{5 \times 10^{14} h^{-1} M_\odot} \right)^\alpha. \quad (15)$$

It has been recently shown that $Y_x = M_g T$ (evaluated within a certain over density, here R_{500}) behaves as a low-scatter proxy for the cluster mass, regardless of the dynamical state of the cluster (e.g., Kravtsov et al. 2006), since it essentially expresses the total thermal energy of the gas which is not strongly affected by cluster mergers.

The parameter $C2$ has the units of $keV M_\odot$. It has been shown that the universal pressure profile is consistent with SZ observations at low redshift (Arnaud et al. 2010). We therefore do not show the scaling law at $z = 0$, but focus on the evolution of the normalization with redshift. Again, the curves in Figure 8 shows the expectations from a self-similarly scaled universal pressure profile (solid line) and those from entropy injection at high redshift with the following scalings: $\propto (1+z)^{0.5}$ (short-dashed line), constant in redshift (long dashed line), and $\propto (1+z)^{-0.5}$ (dot-dashed line). The dotted lines again show the results of three types of simulations mentioned above, without feedback (GO), with AGN/supernova feedback (FO) and with pre-heating (PC), as reported in Short et al. (2010).

5 DISCUSSION

Figure 7 shows that the self-similar evolution of the universal pressure profile (solid line) is consistent with the available data. The case for constant entropy injection (dot-dashed line) and positive evolution do not fare well, and the match with the data improves for negative redshift evolution (dashed line) of entropy injection. As mentioned earlier, the self-similarly scaled universal pressure profile is equivalent to a scaling of entropy injection as $(1+z)^{-0.8}$, and the solid line therefore also shows the case of a steep negative evolution with $\alpha = -0.8$. The results from enhanced entropy are largely consistent with the range of results from current simulations including feedback and preheating (shown by the dotted lines marked as FO and PC).

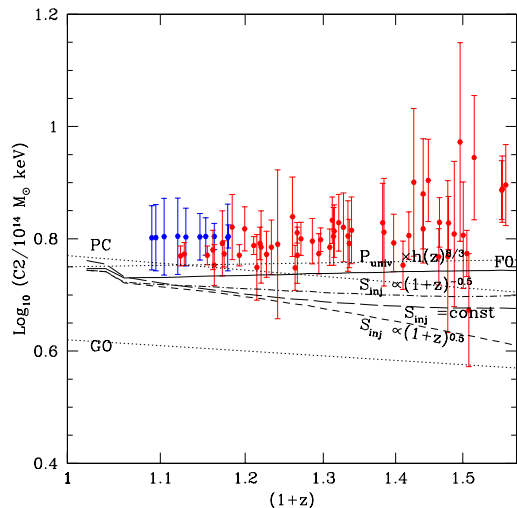


Figure 8. Same as Figure 7, but for the normalization parameter C_2 of $Y_X - M_{500}$ relation. Data points from REXCESS (Pratt et al. 2009) are shown as blue and high redshift data from Maughan et al. (2006) are shown with red points.

The curves in figure 8 show that the self-similar evolution of the universal pressure profile is consistent with the available data, and that the data favour negative evolution of entropy injection in general. The enhanced profile with our simple scaling law are consistent with the results from simulations including feedback. Comparing with the data, which include low-redshift observational data from REXCESS (Pratt et al. 2009; Short et al. 2010) and high redshift data from Maughan et al. (2006), we find that the case of constant entropy injection matches better and, as in the case of $L_x - T$ relation, the situation improves with negative redshift evolution. A more detailed analysis of the likelihood of the values of α that is allowed by the data is beyond the scope of the present paper, and we will pursue this approach in a future paper, and determine the possible evolution of entropy injection, parameterized by certain variables whose values could be determined by comparing with existing data. But the trend shown in Figure 8, indicates that the available data require an evolution of the entropy injection that scales as $(1+z)^\alpha$ with $\alpha \leq -1$. Note that owing to the non-gravitational nature of the feedback processes, the enhanced entropy need not evolve self-similarly with redshift. However, the entropy of gas as determined by gravity alone is expected to evolve self-similarly, namely, $S \propto E(z)^{-2/3}$ for clusters with same mass. Nevertheless, we can compare the entropy scaling inferred above with the self-similar scaling. In Λ -CDM model, $E(z)^{-2/3}$ roughly scales as $(1+z)^{-0.4}$ in this redshift range. Therefore, the scaling $S_{inj} \propto (1+z)^{-1}$ can be written as $S_{inj} \propto E(z)^{-2/3}(1+z)^{0.6}$, which is indicative of a non-standard evolution.

A more important conclusion that we can draw from the previous section, however, is that in the presence of accurately determined cluster scaling relation evolution, as is expected in the near future, one will be able to compare the predictions from entropy injection with that from redshift evolution of cluster scaling relations, and therefore iterate in order to determine the entropy enhancement at high redshift.

Fang & Haiman (2008) have argued, on the basis of a simple model of evolving entropy floors for the ICM with redshift and comparing the results with observed evolution of scaling relations, that the entropy floor at high redshift is likely to be shallower than that at present. They argued that a decreasing entropy floor with redshift is expected from feedback processes due to active galactic nuclei (AGN) and supernovae driven winds.

It is however difficult to interpret the amount of feedback only from the level of the entropy floor, since the default entropy at high redshift is also likely to be small, from cosmological evolution. Entropy, as defined by $S \equiv T/n_e^{2/3}$, would normally evolve as $E(z)^{-2/3}$, for clusters with same virial mass, in the absence of any feedback process. Any deviation from this can be identified as the result of a feedback process. For example, Ettori et al. (2004) found that for clusters with same temperatures, the entropy floor evolves as $E(z)^{4/3} S \propto (1+z)^{0.3}$. Nath (2004) interpreted this as the result of increasing feedback energy deposition at higher redshifts, possibly as a result of increase in the abundance of AGNs at high redshift.

Our work in this paper presents a method of determining the amount of feedback and its evolution with redshift, by using an initial entropy profile and injecting entropy into the profile (defined by radially distributed gas shells). It remains to be seen how the entropy injection prescription is related to any physical process of feedback, and we will return to this issue in a future paper.

Finally, we note that our results are accurate up to $\sim 15\%$, given the accuracy with which we have implemented the boundary conditions in arriving at our results. Our analysis presented here has ignored the contribution from non-thermal pressure of the gas, which can lead to underestimating the mass by $15 - 20\%$ around r_{2500} at $\sim 25\%$ at the virial radius (see for example, Rasia et al. 2004), but which would have introduced additional free parameters, and more uncertainties in the interpretation of cluster scaling relation data, the results of the entropy injection prescription. The simplicity of the entropy injection prescription presented in this paper, however, may make it possible to include non-thermal pressure.

There is another source of uncertainty that arises from the fact that a fraction of the baryons in clusters would form stars, and would thus affect the boundary condition for normalization. Although Gonzalez et al. (2007) found that the stellar mass fraction in a cluster of $M_{500} = 10^{14} M_\odot$ can be as large as $0.25\Omega_b/\Omega_m$ (see also Giodini et al. 2009; Andreon et al. 2010), Balogh et al. (2008) have found that such a large fraction, if confirmed, would cause problem for the paradigm of hierarchical structure formation, let alone being an 'overcooling' problem. On the other hand a conservative estimate from Bower et al. (2006) is that the stellar fraction is ~ 0.1 times the cosmic baryon fraction. This is also in agreement with hydro simulations of clusters (Ettori et al. 2006). Recently, Simionescu et al. (2011) have found from Suzaku observations of the Perseus cluster that the baryon fraction approaches the Universal value much earlier than the virial radius. All of these would imply that our boundary conditions used here would be modified by a factor $\sim (1 - 0.1)$, and the resulting profiles would differ by $\sim 10\%$ and, hence, would decrease the required entropy injection by a similar fraction. We have neglected the contri-

bution of star formation in this paper because our entropy injection prescriptions are accurate up to $\sim 15\%$.

We would like to thank the referee for a very careful reading of the manuscript that has helped us in improving the paper. We thank Satej Khedekar for help with Figures 7 and 8.

REFERENCES

Andreon, S. 2010, *MNRAS*, 407, 263
 Arnaud, M., Pratt, G. W., Piffaretti, R., Boehringer, H., Croston, J. H., Pointecouteau, E. 2010, *A&A*, 517, 92
 Balogh, M. L., Pearce, F. R., Bower, R. G., & Kay, S. T. 2001, *MNRAS*, 326, 1228
 Balogh, M. L., McCarthy, I. G., Bower, R. G., & Eke, V. R. 2008, *MNRAS*, 385, 1003
 Battaglia, N., Bond, J. R., Pfrommer, C., Sievers, J. L., & Sijacki, D. 2010, *ApJ*, 725, 91
 Benson, B. A., Church, S. E., Ade, P. A. R., Bock, J. J., Ganga, K. M., Henson, C. N., & Thompson, K. L., 2004, *ApJ*, 617, 829
 Birkinshaw, M., 1999, *Physics Reports*, 310, 97
 Bonaldi, A., Tormen, G., Dolag, K., & Moscardini, L. 2007, *MNRAS*, 378, 1248
 Bonamente, M., Joy, M., LaRoque, S. J., Carlstrom, J. E., Nagai, D., & Marrone, D. P. 2008, *ApJ*, 675, 106
 Borgani, S., Murante, G., Springel, V., Diaferio, A., Dolag, K., Moscardini, L., Tormen, G., Tornatore, L., & Tozzi, P. 2004, *MNRAS*, 348, 1078
 Branchesi, M., Gioia, I. M., Fanti, C., Fanti, R. 2007, *A&A*, 472, 739
 Bryan, G. L., & Norman, M. L. 1998, *ApJ*, 495, 80
 Chaudhuri, A., & Majumdar, S. 2011, *ApJ*, 728, L41
 Chen, Y., Reiprich, T. H., Böhringer, H., Ikebe, Y., Zhang, Y.-Y. 2007, *A&A*, 466, 805
 Comerford, J. M., Natarajan, P. 2007, *MNRAS*, 379, 190
 da Silva, A. C., Kay, S. T., Liddle, A. R., & Thomas, P. A. 2004, *MNRAS*, 348, 1401
 Ettori, S., Tozzi, P., Borgani, S., Rosati, P. 2004, *A&A*, 417, 13
 Ettori, S., Dolag, K., Borgani, S., & Murante, G., 2006, *MNRAS*, 365, 1021
 Fan, W. & Haiman, Z. 2008, *ApJ*, 680, 200
 Finoguenov A., Reiprich T. H., Böhringer H., 2001, *A&A*, 368, 749
 Giodini, S. et al. 2009, *ApJ*, 703, 982
 Gladders, M. D., et al. . 2007, *ApJ*, 655, 128
 Gonzalez, A. H., Zaritsky, D., Zabludoff, A. I. 2007, *ApJ*, 666, 147
 Hartley, W. G., Gazzola, L., Pearce, F. R., Kay, S. T., Thomas, P. A. 2007, *MNRAS*, 386, 2015
 Hilton, M. et al. 2007, *ApJ*, 670, 1000
 Holder, G., Haiman, Z., & Mohr, J. J., 2001, *ApJ*, 560, L111
 Kravtsov, A. V., Nagai, D., & Vikhlinin, A. A. 2005, *ApJ*, 625, 588
 Kravtsov, Andrey V., Vikhlinin, Alexey, Nagai, Daisuke 2006, *ApJ*, 650, 128
 Li, R., Mo, H. J., Fan, Z., van den Bosch, F. C., Yang, X. 2010, *MNRAS*, (astro-ph/1006.4760)
 Loken C., Norman M. L., Nelson E., Bryan G. L., Motl P., 2002, *ApJ*, 579, 571
 Mazzotta, P., Rasia, E., Moscardini, L. & Tormen, G. 2004, *MNRAS*, 354, 10
 Majumdar, S., & Mohr, J. J., 2003, *ApJ*, 585, 603
 Majumdar, S., & Mohr, J. J., 2004, *ApJ*, 613, 41
 Maughan, B. J., Jones, L. R., Ebeling, H., Scharf, C. 2006, *MNRAS*, 365, 509
 Maughan, B. J. 2007, *ApJ*, 668, 772
 Mitchell, N. L., McCarthy, I. G., Bower, R. G., Theuns, T., Crain, R. A. 2009, *MNRAS*, 395, 180
 Morandi, A., Ettori, S., Moscardini, L. 2007, *MNRAS*, 379, 518
 Muanwong, O., Kay, S. T., Thomas, P. A. 2006, *ApJ*, 649, 640
 Nath, B. B., Roychowdhury, S. 2002, *MNRAS*, 333, 145
 Nath, B. B. 2004, *MNRAS*, 353, 941
 Navarro, J. F., Frenk, C. S., White, S. D. M. 1997, *ApJ*, 490, 493
 Pcaud, F. et al. 2007, *MNRAS*, 382, 1289
 Pointecouteau, E., Arnaud, M., Pratt, G. W. 2005, *A&A*, 435, 1
 Pratt, G. W., Arnaud, M., Piffaretti, R., Boehringer, H., Ponman, T. J., Croston, J. H., Voit, G. M., Borgani, S., Bower, R. G. 2010, *A&A*, 511, 85
 Puchwein, E., Sijacki, D., & Springel, V. 2008, *ApJ*, 687, L53
 Rasia, E., Tormen, G., Moscardini, L. 2004, *MNRAS*, 351, 237
 Rapetti, D., Allen, S. W., Mantz, A., & Ebeling, H., 2009, *MNRAS*, 400, 699
 Rapetti, D., Allen, S. W., Mantz, A., & Ebeling, H., 2010, *MNRAS*, 406, 1796
 Romer, A. K.; Viana, P. T. P., Liddle, A. R., Mann, R. G. 2001, *ApJ*, 547, 594
 Roychowdhury, S., Ruzszkowski, M., Nath, B. B., Begelman, M. C. 2004, *ApJ*, 615, 681
 Roychowdhury, S., Ruzszkowski, M., & Nath, B. B., 2005, *Apj*, 634, 90
 Rozo, E., et al. , 2010, *ApJ*, 708, 645
 Sartoris, B., et al. 2010, *MNRAS*, 407, 2339
 Short, C. J., Thomas, P. A., Young, O. E., Pearce, F. R., Jenkins, A., & Muanwong, O. 2010, *MNRAS*, in press (astro-ph/1002.4539)
 Simionescu, A., et al. 2011, astro-ph/1102.2429
 Sun, M., Voit, G. M., Donahue, M., Jones, C., Forman, W., Vikhlinin, A. 2009, *ApJ*, 693, 1142
 Vikhlinin, A., et al. , 2009, *ApJ*, 692, 1060
 Voit, G. M., Bryan, G. L. 2001, *Nature*, 414, 425
 Voit, G. M. 2005, *Rev. Mod. Phys.*, 77, 207
 Wang, L., & Steinhardt, P. J., 1998, *ApJ*, 508, 483
 White, M., Hernquist, L., & Springel, V., 2002, *ApJ*, 579, 16